Amphiphilic Nanofiber Based Aerogels for Selective Liquid Absorption from Electrospun Biopolymers

Fabian Deuber, Sara Mousavi, Lukas Federer, and Christian Adlhart*

F. Deuber, S. Mousavi, L. Federer, Dr. C. Adlhart
Institute of Chemistry and Biotechnology, Zurich University of Applied Sciences ZHAW, Einsiedlerstrasse 31, 8820 Wädenswil, Switzerland
S. Mousavi
Department of Chemical Engineering, University of Sistan and Baluchestan, Zahedan, Iran
E-mail: christian.adlhart@zhaw.ch

Abstract

Hierarchically structured and ultralight pullulan/PVA aerogels or sponges were prepared from short electrospun nanofibers using solid templating. The architecture of the aerogel consisted of cell-like pores of 50 to 100 μm interconnected by a network of entangled nanofibers with 2 to 5 μm pores. Such structures allow rapid liquid uptake with high liquid holding capacities at the same time. The amphiphilic nature of the aerogel from the electrospun biopolymer was switched by chemical vapor deposition of silane. This allows the selective separation of liquids based on their different relative dielectric constants, which is of high interest for oil spilled waters and produced water. Furthermore, silylation improved the aerogel's overall mechanical stability by 18 % while increasing its density by only 5 %. SEM *in situ* compression studies revealed the importance of the fibrous entanglement and the open-porous architecture for the high bendability and mechanical resilience of the aerogels. Solid templating of short electrospun nanofibers facilitates the design of a fascinating class of ultralight aerogels while prevailing the fibrous character and the versatility of electrospinning.

Introduction

Electrospinning allows the fabrication of nanofibers from biopolymers, synthetic polymers, and even metals. In terms of applications electrospinning has outperformed alternative technologies for nanofiber production such as melt blowing,[1] self-assembly, [2] phase separation,[3] solution blow spinning,[4] and nanofiber drawing.[3a] Electrospun nanofibers feature a large specific surface area, ultra-high aspect ratio, extreme flexibility, and the electrospinning process can easily be scaled up. One limitation in electrospinning is the anisotropic lamellar deposition character due to the layer-by-layer manufacturing process.[5] Different ways to fabricate porous 3D structures from electrospun nanofibers have been exploited,[6] such as self-assembly,[7] cool drum spinning[8] or gas expansion.[9] Even though those 3D scaffolds lack the possibility to add scalable pores and often suffer from poor mechanical stability,[10] the scientific resources devoted to developing electrospun 3D materials are increasing each year.[6b] The unique properties of 3D materials from electrospun nanofibers enable their application as scaffolds in tissue engineering,[11] framework for heterogeneous catalysis,[12] drug release composites,[11c, 13] personal safety equipment,[14] sensors,[15] or electrodes.[16]

It has been shown recently, that colloidal dispersions of short electrospun nanofibers prepared by cutting electrospun membranes open a complementary and controlled approach in nonwoven nanofiber processing.[17] This change in paradigm — to separate fiber formation and fiber processing — elegantly overcomes the main drawback of electrospinning, since fiber processing is no longer coupled to the intrinsically lamellar fiber deposition, but separated into more versatile liquid handling process. Using short electrospun nanofiber dispersions, Ding[5a] and Greiner[18] pioneered the preparation of ultralight 3D aerogels or sponges by freeze casting. These nanofiber based 3D materials are either referred to as aerogels[5a] or sponges[18]. They show high porosities like silica based aerogels, but the solid

scaffold is pre-formed by short nanofibers.[19] Our group rigorously controlled this underlying self-assembly solid templating process to form hierarchically structured nanofiber aerogels with tailored pore size.[20]

We present a simple and efficient route to prepare highly porous interconnected networks of electrospun nanofibers with tailored pore feature. Furthermore, we illustrate the vast potential of post-treating such 3D aerogels: subsequent hydrophobic modification using chemical vapor deposition (CVD) allowed us to alter the inherent characteristics and morphology of the electrospun pullulan/PVA nanofibers within the aerogel. The nanofiber based aerogels in this work were designed to fulfill several criteria. (i) The 3D framework of the aerogel should not collapse during further treatment and thus had to be mechanically resistant. (ii) The structure should display an open cellular architecture and most importantly (iii) the intrinsic properties and shape of the nanofibers - such as large specific surface area and aspect ratio - were retained. By selecting a pullulan/PVA blend as nanofiber starting material, we were able to perform *in situ* crosslinking to ensure high mechanical stability and to increase compression resistance.[21] Furthermore, pullulan — a homopolysaccharide of glucose — is biodegradable, GRAS-approved and amphiphilic, because of the presence of hydrophilic hydroxyls groups and hydrophobic pyranose rings. In contrast to the hydrophobic nanofiber aerogels prepared by Ding[5a, 22] and Greiner,[18, 23] the amphiphilic character of pullulan allows the uptake of both polar and non-polar solvents. Additionally, the presence of ample hydroxyl groups facilitates chemical post modification.[24] We meth the remaining two requirements — hierarchically structured features and the preservation of the characteristics of the nanofibers by using a controlled solid templating technique adapted for short pullulan/PVA nanofibers.

To synthesize the aerogel, see **Figure 1**a, nonwoven nanofiber membranes were first produced by environment-friendly free-surface electrospinning pullulan/PVA from aqueous

solution (see Supporting Information). Electrospinning under benign conditions yielded uniform nanofibers with a diameter of 240 ± 55 nm.[25] The nanofiber membranes were homogenized in 1,4-dioxane to provide a suspension of short nanofibers with a length of approx. 40 μm, and subsequently frozen using a directional solid templating approach.[20, 26] Sublimation by freeze-drying yielded the green bodies — an ultralight (density between 4.1 and 48.2 mg ml^{-1}) and highly porous (porosity up to 99.7 %) fibrous network with directional pores along the thermal freezing gradient. It is so light that a dandelion can carry it without deforming the fluffy seed heads (Figure1b). By carefully controlling both the fiber concentration and the freezing conditions, solid templating showed great flexibility in tailoring both the microstructure and the macrostructure of the architecture of the aerogel (see Supporting Information). The water soluble green bodies were thermally crosslinked at 180 °C for 40 min to render them insoluble. During this thermal process, at least two reactions occur simultaneously: first ether bond formation, which renders the polymers water insoluble, and second carbohydrate oxidation (caramelization) of maltose, a residue from the pullulan production, leaving a brownish hue. Crosslinking of the pullulan/PVA green bodies increased the compressibility and mechanical resistance, but lead to a shrinking between 45 and 65 %, **Table 1**. Crosslinking the water-soluble pullulan/PVA polymer blend is crucial for its application under wet conditions and outweighs the side-effects (shrinking and discoloration) during the thermal crosslinking of the aerogel. Adding supporting inorganic nanofibers such as SiO$_2$ can preserve the initial volume during thermal crosslinking at the cost of the biodegradable properties of the aerogels.[5a, 22] Likewise, using polymeric or inorganic coatings to enhance the stability of the aerogels leads to a loss of the intrinsic surface properties of the fibers.[23]
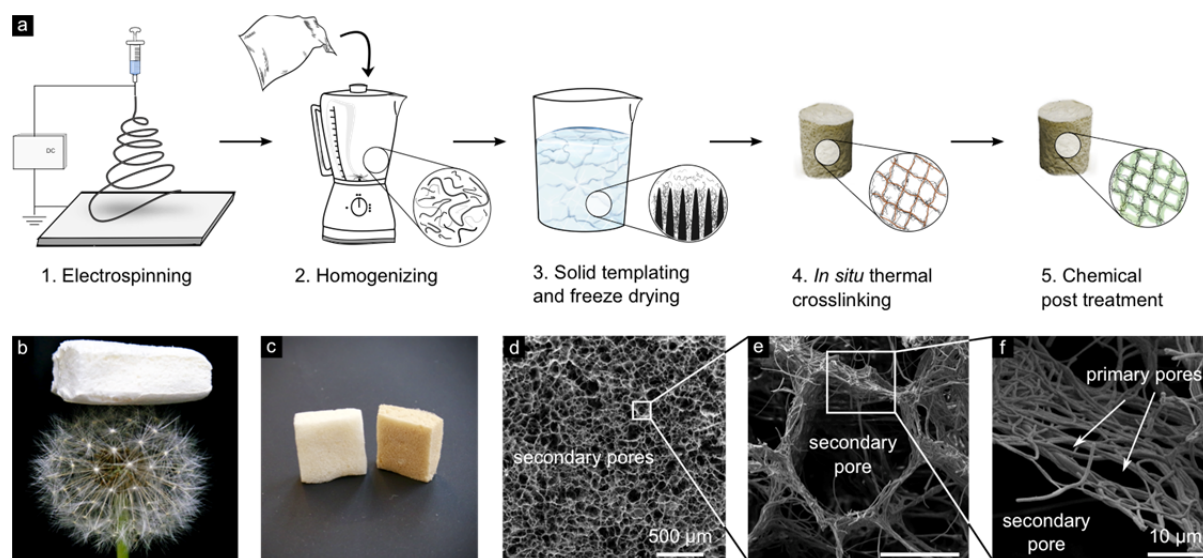
Figure 1. a) Processing steps for the synthesis of 3D electrospun nanofiber based aerogels by freeze-casting: 1.) electrospinning uniform nanofibers, 2.) homogenizing of the electrospun membrane in a wetting non-dissolving liquid to obtain short fibers with a length of approx. 40 µm and an aspect ratio of 120‑150, 3.) solid templating at a controlled rate and successive sublimation of the solidified non-solvent to obtain the free standing green body aerogel, 4.) thermal crosslinking to achieve water insolubility, 5.) hydrophobic modification of the amphiphilic network by CVD with trichloro(octyl)silane (TOS). b) Pullulan/PVA aerogel (apparent density of 8.7 mg ml^{-1}) freestanding on a dandelion without deforming the fluffy seed heads. c) Discoloration associated with crosslinking (left) and post-treatment (right) of the nanofiber aerogel. d) to f) SEM images of a cross-section from a nanofiber-based aerogel perpendicular to the freezing direction showing the hierarchical pore architecture at different magnification. The open pore architecture with major secondary pores between 50-100 µm (d and e) and minor primary pores between 2-5 µm (e) is clearly visible. Notably, the nanofibers' morphology within the aerogel is preserved.

We could modify the amphiphilic framework of the aerogel to selectively absorb non-polar liquids by CVD using trichloro(octyl)silane (TOS). Chemical vapor deposition proved to be an easy but efficient means to render the surface of the fiber hydrophobic without altering the pore structure of the aerogel. The increase in density was only 5 %, regardless of the density of the aerogel before TOS treatment. A slight change in color was observed, see Figure 1c.

Table 1. Archimedean densities of the green body, the crosslinked aerogel, and the post modified silylated aerogel, their Archimedean porosities, and associated volume shrinkage during crosslinking.

Density Green body [mg ml^{-1}]	Porosity Green body [%][a]	Density Crosslinked [mg ml^{-1}]	Porosity Crosslinked [%][a]	Volume Shrinkage [%]	Density Silylated [mg ml^{-1}]	Porosity Silylated [%][a]
4.13	99.72	11.88	99.18	65.2	12.64	99.13

8.78	99.40	23.20	98.40	62.2	24.64	98.31
18.62	98.72	48.91	96.64	61.9	50.84	96.50
48.21	96.68	88.52	93.91	45.6	92.27	93.65

[a]For calculating the porosity see the Supporting Information.

The pore formation process during solid templating is understood by the accepted freezing mechanism for nanoparticle slurries,[27] where the dispersed nanofibers are rejected by the moving solidification front of the growing solvent crystals and thus concentrate between the crystals to form walls of entangled nanofibers separating cellular pores. We could demonstrate that the pore size and shape could be tailored by influencing either the freezing front velocity during freezing or by adjusting the slurry's viscosity through changing the fiber fraction.[5a, 20, 22b] The architecture of the aerogels reveals hierarchical pores: minor primary pores between tangled nanofibers and major cell-like secondary pores. This hierarchical nanostructure and microstructure is clearly visible in SEM images of aerogel cross sections, see Figure 1d to Figure 1e. By zooming in on a major secondary pore, minor primary pores with a size of 2-5 μm are distinctly visible. These primary pores are about the same size as those in electrospun membranes.[15b, 28] A significant difference between these nanofiber based aerogels and conventional cellulose aerogels is the preserved fibrous character within the cell walls despite their ultra-thin dimensions. Typical cellulose aerogels have smooth, regular pore walls, so they are not truly interconnected.[24] Whereas here, the primary pores are interconnected with the larger, secondary pores yielding a truly interconnected, open-pore network of nanofibers. Investigating the sponges with respect to the freezing direction reveals that the secondary pores were aligned parallel to the thermal freezing gradient, see Figure S3. Hence, the aerogel has a hierarchical anisotropic architecture. Such anisotropic properties have been reported many times for ice templated ceramics – both in terms of structure such as strength and E-modulus, but also in terms of function such as thermal conductivity, acoustic properties, or gas permeability.[29] Here, we were interested in thehierarchical pores for

efficient mass transport properties in combination with a large and accessible internal surface provided by the network of entangled nanofibers.

The combination of the robust hierarchical cellular structure and the characteristic entanglement of the fibers may also be responsible for the high bendability and reversible compressibility of the nanofiber aerogels. They are superior to the typically fragile ceramic aerogels, which disintegrate under compression stress.[30] By studying their compression behavior, we found that the aerogels can bear high compression strain, ε, up to 80 % and still recover their original shape. Stress-strain curves display two characteristic regimes: a linear, Hookean regime for $\varepsilon \leq 40$ %, where no plastic deformation occurs, and a densification regime above $\varepsilon \geq 40$ %, see **Figure 2**a. Deformation was also observed by SEM *in situ* compression studies, where the pore walls undergo non-linear compression at high deformation, also known as elastic buckling.[31] We carried out multiple compression cycles, see Figure 2c, and observed a plastic deformation of the structure after the first five compression cycles at a strain of $\varepsilon = 60$ %. However, it is less pronounced for the silylated aerogel, emphasizing the reinforcement through silylation. At reduced compression strain of $\varepsilon = 30$ % the aerogels exhibited almost no deformation and retained their original shape even after 100 cycles, see Figure S6c. The rapid shape recovery of the ultralight aerogel is also observed when wet (see Figure S7). Whereas conventional open-porous foams display failure and plastic deformation due to exhaustive buckling, fibrous aerogel display fatigue residency. Due to the fibrous structure in the pore walls of the aerogels fast energy dispersion throughout the entire structure is ensured. This so-called multi-arch architecture acts as an elastic spring-type cushioning system, minimizing the effect of fatigue failure.[32] This efficient load transfer was observed when studying the open porous aerogel by *in situ* scanning electron microscopy (SEM), see Figure 2e and f.

Youngs' moduli were between 5.1 and 401 kPa depending on the density of the silylated aerogel (from 12.64 to 92.27 mg ml^{-1}). While crosslinking and successive silylation of the aerogel renders the structure non-soluble and hydrophobic, the *E*-modulus depends primarily on the density of the aerogel. Normalized to their density the specific *E*-moduli of the aerogels were within 0.45 and 4.2 MPa ml g^{-1}, thus they are comparable with other solid templated aerogels from electrospun nanofibers.[5a, 18, 22a, 23, 33] Thanks to their highly interconnected fibrous network they exhibit similar properties as carbohydrate aerogels with smooth regular pore walls from cellulose (< 2 MPa ml g^{-1}),[34] or starch (< 10 MPa ml g^{-1}).[35] Carbon aerogels, however, generally show higher specific *E*-moduli (20 MPa ml g^{-1},[36] or even over 330 MPa ml g^{-1},[37]) thus suggesting that pyrolysis of the pullulan/PVA aerogel could potentially improve mechanical properties. Using the model proposed by Gibson and Ashby the architecture of a cellular material can be elucidated, given its scaling behavior of the relative *E*-modulus versus its relative density.[31, 38] When comparing our aerogel structures with selected materials from literature, it becomes apparent that our aerogels behave like open-cell structures, see Figure 2d. Our finding confirms the hypothesis of Ding *et al*.[5a, 22b] and is supported by the SEM *in situ* compression study.
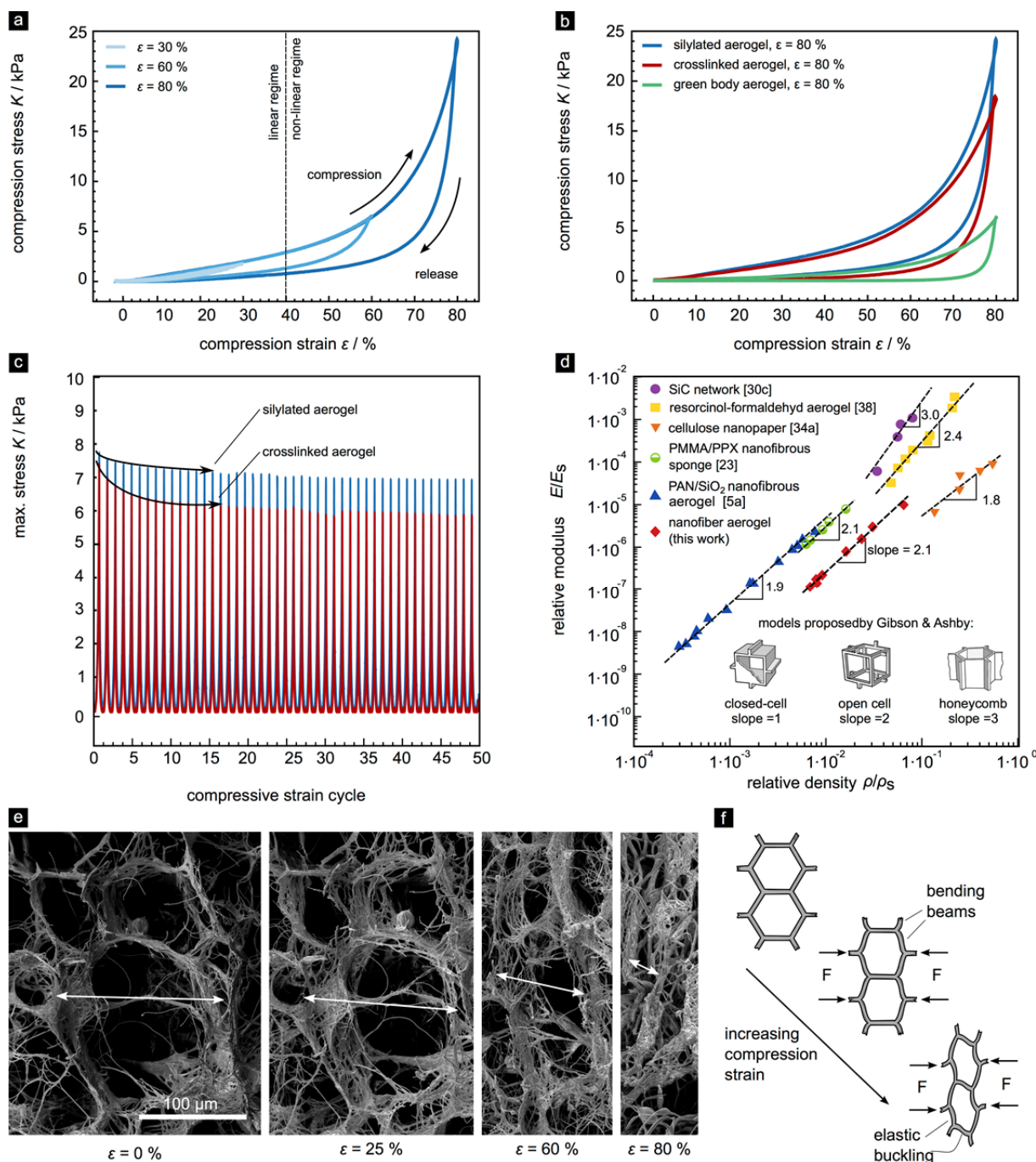
Figure 2. Mechanical properties of the nanofiber based aerogels (green body, crosslinked, and silylated) with an apparent density of 8.78, 23.20, and 24.64 mg ml^{-1}, respectively (Table 1). a) Compression stress, K, versus compression strain ε = 30, 60 and 80 % of the silylated aerogel. b) Comparison of the compression behavior of the aerogel after different processing steps (green body, crosslinked, and silylated). c) First 50 cycles of the fatigue test at a compression strain ε = 60 % illustrating the enforcement by silylation (for 100 cycles see Figure S6). d) Scaling behavior of nanofiber based aerogels with different densities. Literature data:[5a, 23, 30c, 34a, 39] The nanofiber based aerogels from this work show open-cell behavior (slope 2.1). E_s and density ρ_s of the solid were estimated using literature values of pullulan[40] and PVA:[41] $E_{pullulan}$ = 28 GPa, $\rho_{pullulan}$ = 1.85 mg ml^{-1} and E_{PVA} = 46 GPa, ρ_{PVA} = 1.19 mg ml^{-1}, respectively. The pullulan/PVA ratio to calculate the weighted arithmetic mean E-modulus and density of the composite was 2:3. e) SEM *in situ* compression study with

increasing degree of compression (parallel to the freezing direction). The proposed elastic buckling can be observed by following the pore walls of the secondary pores (white arrow). f) Mechanistic scheme for the compression of open-pore structures.

With hydroxyl groups surrounding the hydrophobic pyranose ring, pullulan exhibits similarly to cellulose an affinity to both polar and non-polar solvents. Unmodified but crosslinked pullulan/PVA aerogels with a density of 11.88 mg ml^{-1} absorb due to their amphiphilic nature both water (102.0 m^3 m^{-3}) and chloroform (115.2 m^3 m^{-3}), see **Figure 3**e. The high liquid absorption capacity, φ, concerning the fiber volume, indicates a pore filling mechanism *via* capillary forces, capable of invading up to 100 % of the available free space (total pore volume of 115.6 m^3 m^{-3}). After silylation, water can no longer penetrate but is forming droplets on the aerogel's surface with a contact angle of 136 ° (Figure 3b). When a water drop is touching the hydrophobic surface of the aerogel, it is partially penetrating into the hierarchically structured fibrous topography, allowing the small water drops (5 µl) to adhere to the surface. As shown in Figure 3c, these little water droplets (dyed with methyl blue) do not move — even when rotated upside down — implying the formation of a Cassie impregnating wetting area or a so-called "Gecko"-state.[24d, 42] Simultaneously, hydrophobic silylated pullulan/PVA aerogels rapidly and selectively remove non-polar solvents such as cyclohexane or chloroform from water (Figure 3d and Figure S8). The complete absorption of hydrocarbons from water demonstrates the excellent potential for oil removal, e.g. from produced water. Furthermore, the silylated aerogels display high absorption capacities, φ, towards a wide range of liquids, including aliphatic (cyclohexane, petroleum ether, *n*-hexadecane), polar aprotic (ethyl acetate, 1,4-dioxane), chlorinated (dichloromethane, chloroform) solvents, and silicone oil. When the hydrophobic aerogel is forced into polar solvents such as water, ethylene glycol or dimethyl sulfoxide (DMSO) the liquid is repelled, filling only less than 15 % of the available pore volume. Hence, it is evident, that a higher relative dielectric constant ε_r of a solvent with $\varepsilon_r \geq 37$ correlates with less or no absorption

capacity. By further exploiting the high and tunable porosity of such electrospun nanofiber based aerogels, it is even possible to increase the absorption capacity to almost 430 m^3 m^{-3}.[18]

In summary ultralight (4.13 mg ml^{-1}) and highly porous (99.70 %) nanofiber based aerogels were successfully synthesized using a controlled solid templating approach for short electrospun nanofibers. CVD with TOS was applied to turn the initially amphiphilic pullulan/PVA framework of the aerogel into a hydrophobic one with selective absorption of non-polar solvents. This illustrates the potential of combining two established high impact techniques namely electrospinning and freeze-casting. We expect that thanks to their outstanding mechanical behavior, their large specific surface area, and their tunable microstructure these fascinating nanofiber based aerogels obtained by solid templating will establish in numerous applications: either as filtration and separator structure, as a catalyst support, as dampers and isolators, as pressure sensors, absorbents, or as a scaffold for tissue engineering.
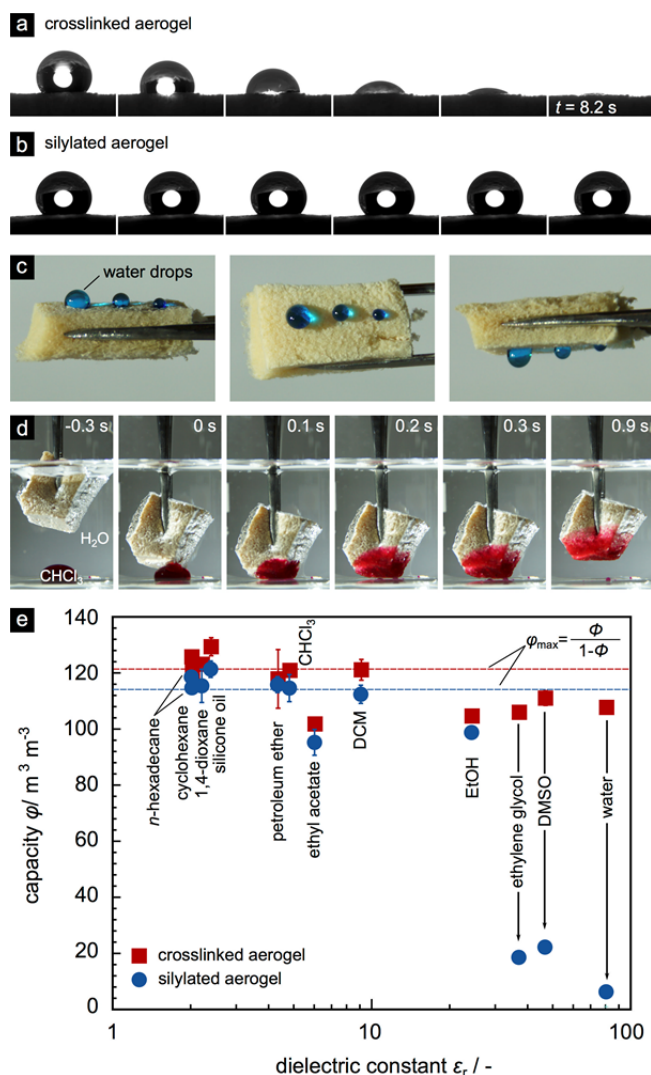
Figure 3. a) Dynamic water absorption of the amphiphilic crosslinked pullulan/PVA aerogel. b) The water contact angle of the hydrophobic silylated aerogel remained at 136 °. c) Demonstration of water adhesion on the silylated aerogel by rotation from 0 to 180 degrees. d) Rapid and selective uptake of a non-polar liquid (chloroform, dyed with Sudan red IV) from water through the silylated aerogel with full absorption within 0.3 s. e) Absorption capacity $\varphi = V_{\text{liquid}} / V_{\text{fiber}}$ of amphiphilic crosslinked and silylated pullulan/PVA aerogels with apparent density of 11.88, and 12.64 mg ml^{-1}, respectively (Table 1). The dashed lines represent the maximum absorption capacity, φ_{max}, assuming 100 % pore filling

Experimental Section

Preparation of pullulan/PVA aerogels: The Pullulan/PVA composite nanofibers were

prepared by dissolving 4 g Pullulan (food grade, Hayashibara co. Ltd, Japane) and 6 g PVA

(Mw = 89000–98000 Da, DH = 99 %, Sigma-Aldrich) in 90 g Water. Electrospun nanofiber

membranes were obtained by free liquid surface electrospinning with a Nanospider™ NS lab

500 from Elmarco. The fibers were spun at a high voltage of 80 kV using a cylindrical

electrode and a collector distance of 16 cm. Temperature and relative humidity during

electrospinning were 26 ± 3 °C and 26 ± 4 %, respectively. In a typical experiment for the fabrication of nanofiber based aerogels with an apparent density of 8.78 mg ml^{-1}, the nanofiber membrane was cut into small pieces of approx. 1 x 1 cm^2 and dispersed in 100 ml 1,4-dioxane by an IKA T25 homogenizer for 20 min at 13000 rpm. The homogenous dispersion was subsequently poured into a mold and frozen at a specific rate (here 10.29 μm s^{-1}). The frozen solid was then freeze-dried for 48 h and finally thermally crosslinked at a temperature of 180 °C for 40 min. To obtain hydrophobically modified aerogels by chemical vapor deposition using TOS (purity = 97 %, Sigma-Aldrich), a glass container containing TOS was placed together with the crosslinked pullulan/PVA aerogel in a closed desiccator. After 24 h of reaction time at ambient temperature, the surface modified aerogel was subsequently placed under vacuum (10 mbar, 2 hours) to eliminate the excess silane and the coupling product HCl.

Supporting Information
Supporting Information providing details on the electrospinning process, the solid templating conditions, thermal crosslinking, and physical chemical characterization of the aerogels is available from the Wiley Online Library or from the authors.

Received: ((will be filled in by the editorial staff))
Revised: ((will be filled in by the editorial staff))
Published online: ((will be filled in by the editorial staff))

References

[1]   M. A. Hassan, B. Y. Yeom, A. Wilkie, B. Pourdeyhimi, S. A. Khan, *J. Membr. Sci.* **2013**, *427*, 336.
[2]   J. D. Hartgerink, E. Beniash, S. I. Stupp, *Science* **2001**, *294*, 1684.
[3]   a) Y. Z. Zhang, C. T. Lim, S. Ramakrishna, Z. M. Huang, *J. Mater. Sci. - Mater. Med.* **2005**, *16*, 933; b) F. Yang, R. Murugan, S. Ramakrishna, X. Wang, Y. X. Ma, S. Wang, *Biomaterials* **2004**, *25*, 1891.

[4]   a) E. S. Medeiros, G. M. Glenn, A. P. Klamczynski, W. J. Orts, L. H. C. Mattoso, *J. Appl. Polym. Sci.* **2009**, *113*, 2322; b) A. M. Behrens, B. J. Casey, M. J. Sikorski, K. L. Wu, W. Tutak, A. D. Sandler, P. Kofinas, *ACS Macro Lett.* **2014**, *3*, 249.

[5]   a) Y. Si, J. Yu, X. Tang, J. Ge, B. Ding, *Nat. Commun.* **2014**, *5*, 5802; b) W. E. Teo, S. Ramakrishna, *Nanotechnology* **2006**, *17*, R89; c) J. H. Wendorff, S. Agarwal, A. Greiner, *Electrospinning: Materials, Processing, and Applications*, Wiley-VCH, Weinheim, **2012**; d) A. Greiner, J. H. Wendorff, *Angew. Chem. Int. Ed.* **2007**, *46*, 5670; e) R. Buttiker, J. Ebert, C. Hinderling, C. Adlhart, *Chimia* **2011**, *65*, 182.

[6]   a) B. Sun, Y. Z. Long, H. D. Zhang, M. M. Li, J. L. Duvail, X. Y. Jiang, H. L. Yin, *Prog. Polym. Sci.* **2014**, *39*, 862; b) B. Sun, X.-J. Jiang, S. Zhang, J.-C. Zhang, Y.-F. Li, Q.-Z. You, Y.-Z. Long, *J. Mater. Chem. B* **2015**, *3*, 5389.

[7]   a) B. Sun, Y.-Z. Long, F. Yu, M.-M. Li, H.-D. Zhang, W.-J. Li, T.-X. Xu, *Nanoscale* **2012**, *4*, 2134; b) X. Guo, Y. Yao, T. Zhou, R. Xiang, M. Chen, *J. Appl. Polym. Sci.* **2015**, *133*, 43003; c) G. Chang, X. Zhu, A. Li, W. Kan, R. Warren, R. Zhao, X. Wang, G. Xue, J. Shen, L. Lin, *Mater. Des.* **2016**, *97*, 126.

[8]   M. Simonet, O. D. Schneider, P. Neuenschwander, W. J. Stark, *Polym. Eng. Sci.* **2007**, *47*, 2020.

[9]   J. Jiang, M. A. Carlson, M. J. Teusink, H. Wang, M. R. MacEwan, J. Xie, *ACS Biomater. Sci. Eng.* **2015**, *1*, 991.

[10]   J. Rnjak-Kovacina, A. S. Weiss, *Tissue Eng., Part B* **2011**, *17*, 365.

[11]   a) H. Yoshimoto, Y. M. Shin, H. Terai, J. P. Vacanti, *Biomaterials* **2003**, *24*, 2077; b) W. J. Li, C. T. Laurencin, E. J. Caterson, R. S. Tuan, F. K. Ko, *J. Biomed. Mater. Res.* **2002**, *60*, 613; c) M. Goldberg, R. Langer, X. Jia, *J. Biomater. Sci., Polym. Ed.* **2007**, *18*, 241; d) S. Agarwal, J. H. Wendorff, A. Greiner, *Polymer* **2008**, *49*, 5603.

[12]   a) X. Lu, C. Wang, Y. Wei, *Small* **2009**, *5*, 2349; b) E. Formo, E. Lee, D. Campbell, Y. N. Xia, *Nano Lett.* **2008**, *8*, 668; c) G. F. J. Müller, M. Stürzel, R. Mülhaupt, *Adv. Funct. Mater.* **2014**, *24*, 2860.

[13]   T. J. Sill, H. A. von Recum, *Biomaterials* **2008**, *29*, 1989.

[14]   a) R. Gopal, S. Kaur, Z. Ma, C. Chan, S. Ramarishna, T. Matsuura, *J. Membr. Sci.* **2006**, *281*, 581; b) R. S. Barhate, S. Ramakrishna, *J. Membr. Sci.* **2007**, *296*, 1.

[15]   a) X. Y. Wang, C. Drew, S. H. Lee, K. J. Senecal, J. Kumar, L. A. Sarnuelson, *Nano Lett.* **2002**, *2*, 1273; b) Z.-M. Huang, Y. Z. Zhang, M. Kotaki, S. Ramakrishna, *Compos. Sci. Technol.* **2003**, *63*, 2223; c) D. Li, Y. L. Wang, Y. N. Xia, *Adv. Mater.* **2004**, *16*, 361.

[16]   a) V. Thavasi, G. Singh, S. Ramakrishna, *Energy Environ. Sci.* **2008**, *1*, 205; b) X. Chen, S. Xu, N. Yao, Y. Shi, *Nano Lett.* **2010**, *10*, 2133; c) H. Wu, L. Hu, M. W. Rowell, D. Kong, J. J. Cha, J. R. McDonough, J. Zhu, Y. Yang, M. D. McGehee, Y. Cui, *Nano Lett.* **2010**, *10*, 4242.

[17]   a) J. S. Kim, D. H. Reneker, *Polym. Compos.* **1999**, *20*, 124; b) M. Thieme, S. Agarwal, J. H. Wendorff, A. Greiner, *Polym. Adv. Technol.* **2009**, n/a; c) S. Jiang, G. Duan, J. Schöbel, S. Agarwal, A. Greiner, *Compos. Sci. Technol.* **2013**, *88*, 57; d) M. Langner, A. Greiner, *Macromol. Rapid Commun.* **2016**, *37*, 351.

[18]   G. Duan, S. Jiang, V. Jérôme, J. H. Wendorff, A. Fathi, J. Uhm, V. Altstädt, M. Herling, J. Breu, R. Freitag, S. Agarwal, A. Greiner, *Adv. Funct. Mater.* **2015**, *25*, 2850.

[19]   S. Jiang, G. Duan, U. Kuhn, M. Morl, V. Altstadt, A. L. Yarin, A. Greiner, *Angew Chem Int Ed Engl* **2017**, *56*, 3285.

[20]   F. Deuber, S. Mousavi, M. Hofer, C. Adlhart, *ChemistrySelect* **2016**, *1*, 5595.

[21]   S. Islam, S. Rahaman, J. H. Yeum, *Carbohydr. Polym.* **2015**, *115*, 69.

[22]   a) Y. Si, Q. Fu, X. Wang, J. Zhu, J. Yu, G. Sun, B. Ding, *ACS Nano* **2015**, *9*, 3791; b) Y. Si, X. Wang, C. Yan, L. Yang, J. Yu, B. Ding, *Adv. Mater.* **2016**, *28*, 9512.

[23]   G. Duan, S. Jiang, T. Moss, S. Agarwal, A. Greiner, *Polym. Chem.* **2016**, *7*, 2759.

[24]   a) F. Jiang, Y.-L. Hsieh, *J. Mater. Chem. A* **2014**, *2*, 6337; b) X. Yao, W. Yu, X. Xu, F. Chen, Q. Fu, *Nanoscale* **2015**, *7*, 3959; c) R. Lin, A. Li, T. Zheng, L. Lu, Y. Cao, *RSC Adv.* **2015**, *5*, 82027; d) H. Zhang, Y. Li, Y. Xu, Z. Lu, L. Chen, L. Huang, M. Fan, *Phys. Chem. Chem. Phys.* **2016**, *18*, 28297; e) Q. Liao, X. Su, W. Zhu, W. Hua, Z. Qian, L. Liu, J. Yao, *RSC Adv.* **2016**, *6*, 63773.

[25]   F. Deuber, C. Adlhart, *NART 2015-Nanofibers, Applications and Related Technologies* **2015**, 29.

[26]   a) Y. F. Tang, K. Zhao, J. Q. Wei, Y. S. Qin, *J. Eur. Ceram. Soc.* **2010**, *30*, 1963; b) L. Hu, C.-A. Wang, Y. Huang, C. Sun, S. Lu, Z. Hu, *J. Eur. Ceram. Soc.* **2010**, *30*, 3389; c) T. Fukasawa, Z. Y. Deng, M. Ando, T. Ohji, S. Kanzaki, *J. Am. Ceram. Soc.* **2002**, *85*, 2151.

[27]   a) T. Fukasawa, Z. Y. Deng, M. Ando, T. Ohji, Y. Goto, *J. Mater. Sci.* **2001**, *36*, 2523; b) K. Araki, J. W. Halloran, *J. Am. Ceram. Soc.* **2005**, *88*, 1108; c) N. O. Shanti, K. Araki, J. W. Halloran, *J. Am. Ceram. Soc.* **2006**, *89*, 2444; d) S. Deville, E. Saiz, R. K. Nalla, A. P. Tomsia, *Science* **2006**, *311*, 515; e) S. Deville, *Adv. Eng. Mater.* **2008**, *10*, 155; f) W. L. Li, K. Lu, J. Y. Walz, *Int. Mater. Rev.* **2013**, *57*, 37; g) Y. Zhou, S. Fu, Y. Pu, S. Pan, A. J. Ragauskas, *Carbohydr. Polym.* **2014**, *112*, 277.

[28]   D. Li, M. W. Frey, Y. L. Joo, *J. Membr. Sci.* **2006**, *286*, 104.

[29]   a) S. Deville, *Freezing Colloids: Observations, Principles, Control, and Use*, Springer, Cham, Switzerland, **2017**; b) J. Seuba, S. Deville, C. Guizard, *Sci. Technol. Adv. Mat.* **2016**, accepted manuscript.

[30]   a) N. Kranzlin, M. Niederberger, *Adv. Mater.* **2013**, *25*, 5599; b) X. Y. Zheng, H. Lee, T. H. Weisgraber, M. Shusteff, J. DeOtte, E. B. Duoss, J. D. Kuntz, M. M. Biener, Q. Ge, J. A. Jackson, S. O. Kucheyev, N. X. Fang, C. M. Spadaccini, *Science* **2014**, *344*, 1373; c) C. Ferraro, E. Garcia-Tuñon, V. G. Rocha, S. Barg, M. D. Fariñas, T. E. G. Alvarez-Arenas, G. Sernicola, F. Giuliani, E. Saiz, *Adv. Funct. Mater.* **2016**, *26*, 1636; d) J. Seuba, S. Deville, C. Guizard, A. J. Stevenson, *Sci. Rep.* **2016**, *6*, 24326.

[31]   M. F. Ashby, R. F. M. Medalist, *Metall. Trans. A* **1983**, *14*, 1755.

[32]   H. L. Gao, Y. B. Zhu, L. B. Mao, F. C. Wang, X. S. Luo, Y. Y. Liu, Y. Lu, Z. Pan, J. Ge, W. Shen, Y. R. Zheng, L. Xu, L. J. Wang, W. H. Xu, H. A. Wu, S. H. Yu, *Nat. Commun.* **2016**, *7*, 12920.

[33]   a) W. Chen, J. Ma, L. Zhu, Y. Morsi, H. Ei-Hamshary, S. S. Al-Deyab, X. Mo, *Colloids Surf., B* **2016**, *142*, 165; b) W. Chen, S. Chen, Y. Morsi, H. El-Hamshary, M. El-Newhy, C. Fan, X. Mo, *ACS Appl. Mater. Interfaces* **2016**, *8*, 24415.

[34]   a) H. Sehaqui, Q. Zhou, O. Ikkala, L. A. Berglund, *Biomacromolecules* **2011**, *12*, 3638; b) C. Wang, Y. Xiong, B. Fan, Q. Yao, H. Wang, C. Jin, Q. Sun, *Sci. Rep.* **2016**, *6*, 32383.

[35]   a) J. Li, T. Ye, B. Zhou, B. Li, *RSC Adv.* **2014**, *4*, 22251; b) Z. Y. Wu, C. Li, H. W. Liang, J. F. Chen, S. H. Yu, *Angew. Chem. Int. Ed.* **2013**, *52*, 2925.

[36]   Y.-Q. Li, Y. A. Samad, K. Polychronopoulou, K. Liao, *ACS Sustainable Chem. Eng.* **2015**, *3*, 1419.

[37]   H. Huang, P. Chen, X. Zhang, Y. Lu, W. Zhan, *Small* **2013**, *9*, 1397.

[38]   L. J. Gibson, *Mater. Sci. Eng., A* **1989**, *110*, 1.

[39]   R. W. Pekala, C. T. Alviso, J. D. Lemay, *J. Non-Cryst. Solids* **1990**, *125*, 67.

[40]   T. Diab, C. G. Biliaderis, D. Gerasopoulos, E. Sfakiotakis, *J. Sci. Food Agric.* **2001**, *81*, 988.

[41]   T. Peijs, R. J. M. van Vught, L. E. Govaert, *Composites* **1995**, *26*, 83.

[42]   a) S. Wang, L. Jiang, *Adv. Mater.* **2007**, *19*, 3423; b) A. K. Kota, Y. Li, J. M. Mabry, A. Tuteja, *Adv. Mater.* **2012**, *24*, 5838.

Solid templating is the gate to the world of hierarchically structured nanofiber based aerogels. These ultralight pullulan/PVA based materials rapidly absorb the 100 fold amount of liquid thanks to their highly porous architecture. The amphiphilic absorption characteristics were tuned for the selective removal of non-polar liquids from water by post surface modification.

F. Deuber, S. Mousavi, L. Federer, Dr. C. Adlhart *

Amphiphilic Nanofiber Based Aerogels for Selective Liquid Absorption from Electrospun Biopolymers